Effect of Polytetrafluorethylene Content in Fe—N—C-Based Catalyst Layers of Gas Diffusion Electrodes for HT-PEM Fuel Cell Applications

Tanja Zierdt,*[a, c] Julia Müller-Hülstede,[a] Henrike Schmies,[a] Dana Schonvogel,[a] Peter Wagner,[a] and K. Andreas Friedrich[b, c]

Fe-N-C catalysts are a promising alternative to replace cost-intensive Pt-based catalysts in high temperature polymer electrolyte membrane fuel cell (HT-PEMFC) electrodes. However, the electrode fabrication needs to be adapted for this new class of catalysts. In this study, gas diffusion electrodes (GDEs) are fabricated using a commercial Fe-N-C catalyst and different polytetrafluorethylene (PTFE) binder ratios, varying from 10 to 50 wt% in the catalyst layer (CL). The oxygen reduction reaction performance is investigated under HT-PEMFC conditions (160 °C, conc. H_3PO_4 electrolyte) in a half-cell setup. The

acidophilic character of the Fe—N—C catalyst leads to intrusion of phosphoric acid electrolyte into the CL. The strength of the acid penetration depends on the PTFE content, which is visible via the contact angles. The 10 wt% PTFE GDE is less capable to withdraw product water and electrolyte and results into the lowest half-cell performance. Higher PTFE contents counterbalance the acid drag into the CL and impede flooding. The power density at around 130 mA $mg_{Catalyst}^{-2}$ increases by 34% from 10 to 50 wt% PTFE.

Introduction

The high temperature polymer electrolyte membrane fuel cell (HT-PEMFC) operating at temperatures of around 160 °C is a promising technology for heavy-duty and high-power applications.[1] The electrodes of the HT-PEMFC are usually based on Pt, but phosphate ions from the phosphoric acid doped polybenzimidazole membrane can partly poison the Pt surface.[2] This usually requires higher Pt loadings up to 1 mg_{Pt} cm^{-2} per electrode, which comes along with higher material costs in comparison to lower Pt loadings of approx. 0.4 mg_{Pt} cm^{-2} for low temperature (LT)-PEMFCs.[2]

Metal-nitrogen-carbon (M-N-C) catalysts are promising candidates for replacing expensive and rare Pt for catalyzing the

oxygen reduction reaction (ORR) at the cathode.[1] Fe-N-Cs currently represent the most common type of M—N—C catalysts and can significantly reduce the material costs of PEMFCs.[1] They have shown comparable ORR activity to Pt/C in acidic electrolyte.[3] Also, Fe-N-Cs are not affected by phosphate poisoning, it is even assumed that phosphate ions adsorption next to active sites promote ORR by suppling protons, contrary to Pt-based catalysts.[1,4]

However, Fe—N—C catalyst have different properties compared to the well-known Pt catalysts. First, they have a lower volumetric activity compared to Pt-based catalysts, so that thicker CLs are used which can negatively affect the mass transport of reactants.[2] Second, the active $Fe-N_x$-sites are mainly incorporated inside meso- and micropores of the carbon support compared to Pt nanoparticles which are likely deposited in large mesopores and macropores.[5] Depending on the CL structure and wettability properties it is on the one hand possible that $Fe-N_x$-sites located in small micropores become less accessible for oxygen, because the electrolyte floods the pores, as demonstrated by Bevilacqua et al. On the other hand, inaccessible $Fe-N_x$ sites cannot contribute to the ORR.[5a] Third, Fe—N—Cs have an acidophilic character due to $Fe-N_x$- and N-functionalities.[6] These functional groups can be protonated in an acidic environment leading to acid drag into the CL due to ionic interaction with phosphate anions.[6–7] As the characteristics of Fe-N-C catalyst are substantially different from Pt-based catalyst the requirements of electrode composition cannot be transferred. However, electrode constitution in which significant part of the active sides are connected to thin film of phosphoric acid but the pores are effective for gas transport is crucial for the HT-PEMFC performance.[6] Thus, the acidophilic character of the Fe-N-C catalyst demands investigations of CL properties with regard to the wettability. Polytetrafluorethylene (PTFE) is

[a] T. Zierdt, Dr. J. Müller-Hülstede, Dr. H. Schmies, Dr. D. Schonvogel, P. Wagner
Institute of Engineering Thermodynamics
German Aerospace Center (DLR)
Carl-von-Ossietzky-Str. 15, 26129 Oldenburg (Germany)

[b] Prof. Dr. K. A. Friedrich
Institute of Engineering Thermodynamics
German Aerospace Center (DLR)
Pfaffenwaldring 38–40, 70569 Stuttgart (Germany)

[c] T. Zierdt, Prof. Dr. K. A. Friedrich
Institute for Building Energetics, Thermotechnology and Energy Storage (IGTE)
University of Stuttgart
Pfaffenwaldring 31, 70569 Stuttgart (Germany)
E-mail: tanja.zierdt@dlr.de

ChemElectroChem

Research Article
doi.org/10.1002/celc.202300583

**Chemistry
Europe**
European Chemical
Societies Publishing

commonly used as binder in CL, also in Pt-based HT-electrodes, to introduce mechanical stability and a hydrophobic property to the electrodes. Its content in the CL affects the wettability with phosphoric acid, which influences the proton and gas transport.[5a,8]

The role of PTFE for Pt-based cathodes was frequently studied in the last decade with contents varying between 0–60 wt%. There the optimum PTFE content in terms of wettability and performance for HT-PEM Pt-based cathodes was reported to be between 5–20 wt%, depending on parameters like electrode fabrication method, GDL/MPL type, type of catalyst, ink composition, thermal treatment and preparation.[8a,9] Systematical investigation of different PTFE contents in Fe-N-C-based GDEs is not reported yet, although the principle use of Fe-N-C as cathode catalyst in HT-PEMFCs was demonstrated in several studies.[2,5a,7a,10] Strongly deviating PTFE contents of 7 wt%,[5a] 20 wt%,[10e] 25 wt%,[10d] 40 wt%[2,7a] for Fe-N-C-based GDEs were used. In our recent HT-PEMFC study we discovered a continuous voltage increase of Pt/Fe-N-C hybrid cathode electrodes over a duration of 240 hours compared to the Pt-based electrodes which have shown steady operating conditions after few hours.[7b] This demonstrates the demand for GDE optimization and further understanding of electrolyte distribution in Fe-N-C containing electrodes.

Thus, this study reports the effect of different PTFE contents of 10, 20, 40 and 50 wt% in the Pt-free CL on the GDE performance. Contact angles using water and phosphoric acid (conc. H_3PO_4) are determined to compare the wettability of the GDEs. Micro-computed tomography (μ-CT) and energy-dispersive X-ray spectroscopy (EDS) analysis with scanning electron microscopy (SEM) give insights into the catalyst layer morphol-

ogy and composition. Electrochemical half-cell tests applying HT-PEMFC conditions (160 °C, conc. H_3PO_4) are carried out to examine GDE performances. The physical properties of the CL are correlated to the electrochemical ORR performance of the GDEs.

Results and discussion

Morphology and composition of the CL

GDEs with a PTFE content of 10, 20, 40 and 50 wt% PTFE in the CL were fabricated, and the morphological and electrochemical characteristics as well as GDE wettability investigated. For fabrication of the GDEs via ultra-sonic spray coating the ink consisted of a commercial Fe-N-C (PMF-0011904, Pajarito Powder), 2-propanol, ultrapure water and the specific PTFE amounts. A loading of 3 $mg_{Catalyst}\,cm^{-2}$ was targeted for all PTFE contents. First, the catalyst loadings of Fe–N–C-based GDEs with different PTFE contents can be compared. Figure 1-A shows that determining the catalyst loading via ICP-MS or by weighing the electrode before and after coating results in comparable values, while ICP-MS analysis tend to slightly higher loadings. The gravimetric Fe-N-C loading was 2.3, 3.0, 2.4, 2.6 $mg_{Catalyst}\,cm^{-2}$ for the 10, 20, 40 and 50 wt% PTFE GDEs, respectively. The standard deviation of the gravimetric determined loading is in the same range as the precision of the balance. The results are reproduced within a second batch for the 20 wt% PTFE GDE, slight variances are possible as the hygroscopic GDE material can absorb ambient moisture. To reduce this effect, the GDEs were stored under nitrogen
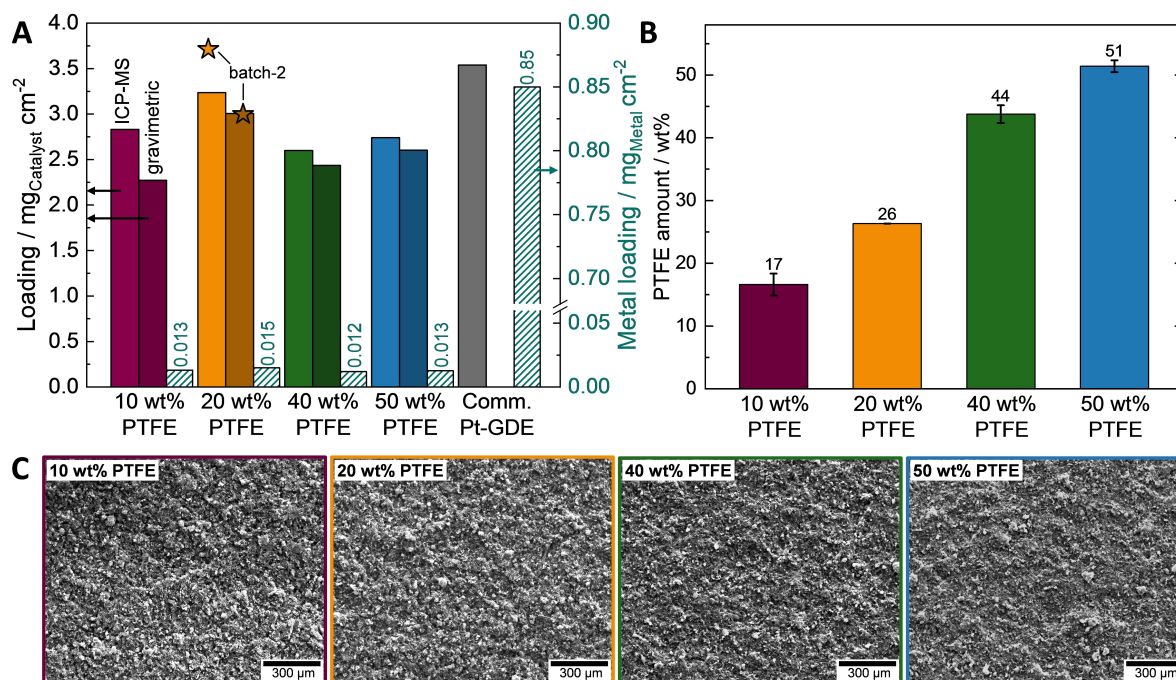

Figure 1. (A) Determination of catalyst loadings via ICP-MS and by gravimetric analysis (left axis), where the catalyst loading of the commercial Pt-GDE is determined by ICP-MS. Metal loading via ICP-MS (right axis) as hatched bars. (B) Calculated PTFE amount from EDS analysis of the CL surface, assuming 2/3 fluorine amount in PTFE (C_2F_4 composition). (C) SEM micrographs of the GDEs with different PTFE contents.

ChemElectroChem

Research Article
doi.org/10.1002/celc.202300583

Chemistry Europe
European Chemical
Societies Publishing

atmosphere until use. The loading was additionally determined by fully quantitative ICP-MS investigation. The ICP-MS analysis Fe-N-C loadings for 10, 20 (batch-1), 20, (batch-2), 40 and 50 wt% PTFE GDEs are 2.8, 3.2, 3.7, 2.6 and 2.7 $mg_{Catalyst}\,cm^{-2}$. Differences between ICP-MS and gravimetric loading can occur. The gravimetric loading is determined non-destructively of the whole 25 cm^2 GDE area, while a size of 1 cm^2 of the GDEs is digested for ICP-MS. These two methods are complementary analyses of catalyst loadings of the GDEs. As a comparison the total catalyst loading of a commercial Celtec® Pt-based GDE a Pt/C loading of 3.5 $mg_{Catalyst}\,cm^{-2}$ was analyzed. The Fe–N–C catalyst itself has an iron content of 0.5 wt_{Fe}% ascertained by ICP-MS measurement. In comparison the commercial Pt-based catalyst has a platinum content of 24 wt_{Pt}%.[11] This leads to a huge difference in the amount of metal in the CL, which can be seen in Figure 1-A. Of course, iron itself is not ORR active, but this comparison reveals the lower active site density of Fe–N–C catalysts compared to Pt-based catalysts, since the active sites of Pt metal nanoparticles are substantially different compared to nitrogen-coordinated single iron metal atoms in the carbon structure.[3b] This affects the required amount of catalyst material for the CL to achieve sufficient performance compared to Pt-based GDEs and thus influences the CL thickness.

Figure 1-B depicts the PTFE content, which was calculated from the detected fluorine amount from EDS mapping. An amount of 2/3 of fluorine in PTFE (C_2F_4 composition) is assumed for each electrode. Increasing PTFE amounts from 10 to 50 wt% are achieved. The PTFE content for the 10 and 20 wt% PTFE is higher than expected. One reason for the difference could be that the X-ray does not penetrate the whole CL, so that the fluorine content of the first few µm of the surface of the CL only is examined. The measured fluorine amount is between 5.5 and 6.8 wt% higher than expected for each sample and probably caused by the overlapping X-ray peaks of iron (0.705 keV) and fluorine (0.677 keV). Iron peaks (0.705 keV, 6.404 keV) were detected within the emission spectra, but quantitative analysis

is inapplicable due to the low iron content resulted in low intensity. The SEM images in Figure 1-C show a porous surface with a homogenous catalyst and PTFE distribution of the CL as revealed by EDS mapping for each PTFE content. EDS-Spectra, C- and F-mappings can be found in the supporting information in Figure S. 1. An attempt to fabricate a GDE with 67 wt% PTFE was unfeasible due to significant sedimentation of the catalyst suspension. Based on this observation, slight sedimentation of the catalyst suspension during coating could be assumed (not visible) for the GDEs with 10–50 wt% PTFE. This might be a reason for some slight differences between the catalyst loadings. Nevertheless, the fabrication of homogenous CLs with a comparable catalyst loading and different PTFE contents was achieved.

In Figure 2 reconstructed 2D images from µ-CT analysis provide insight to the GDE morphology, where the contrast is gained by the different densities of the components. 3D images of the GDE can be found in Figure S. 2 in the supporting information. The PTFE is homogeneously distributed inside the CLs of all GDEs because no thick PTFE agglomerates are visible in the images. The material density can be estimated by the grey scale, because a darker shade is correlated to a higher density.[11–12] The hydrophobic binder PTFE is typically used in the MPL and/or GDL in the range of 0 to 50 wt%[1,13] In Figure 2-A, the MPL appears the darkest along all GDE samples, which can be attributed to a high PTFE content (40 wt% PTFE in MPL[13]). The density of the 40 and 50 wt% PTFE CL appears similar to the density of the MPL as they have a similar darkness. It is also visible, that with increased PTFE content the CL becomes darker. This indicated a denser CL with increased PTFE content.

Figure 2-B presents the CL thicknesses, which was determined at 20 positions at two representative GDE cross sections by subtracting the thickness of the GDL/MPL (determined without the presence of the CL) from the GDE thickness. The percent porosity was determined as the volume of pores as a
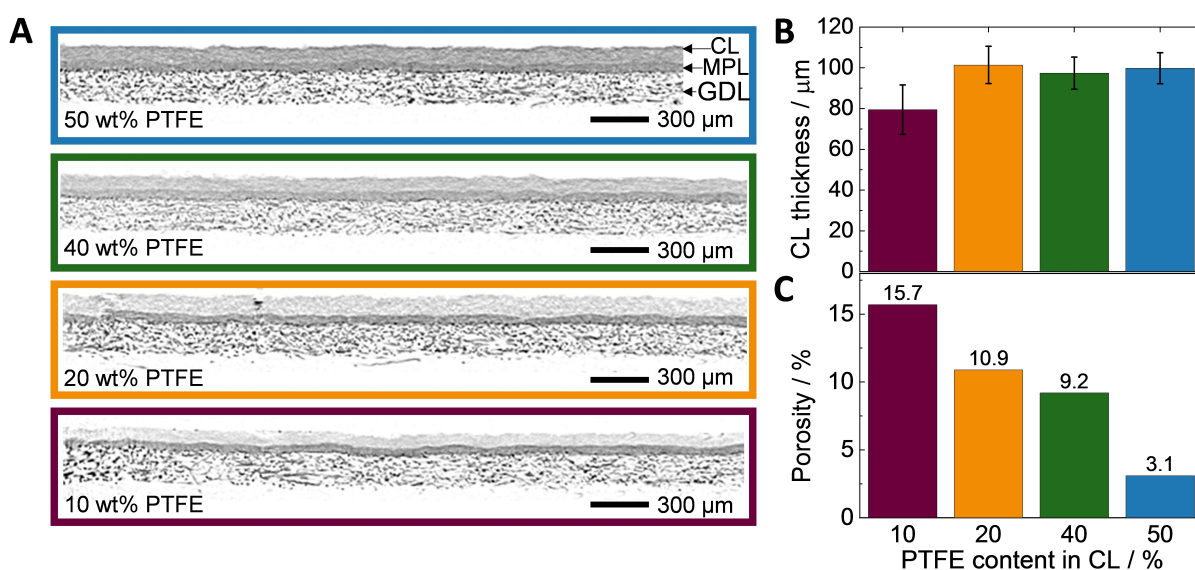

Figure 2. (A) 2D cross-sectional images from µ-CT analysis, (B) measured CL thicknesses, (C) CL porosities.

ChemElectroChem

Research Article
doi.org/10.1002/celc.202300583

**Chemistry
Europe**
European Chemical
Societies Publishing

percent of the total of solid plus the pore volume in the analyzed sample volume. The results are plotted in Figure 2-C. Due to limited resolution of μ-CT (1.9 μm pxl^{-1}) only large macropores are captured as porosity. Retaining the catalyst loading of the Fe-N-C GDEs in a comparable range to the commercial GDE resulted in following CL thicknesses. The GDEs with 20, 40 and 50 wt% PTFE reveal a similar thickness of 100 ± 8 μm, whereas the GDE with 10 wt% PTFE has a thinner CL thickness of 80 ± 12 μm. For the commercial Pt-based GDE a CL thickness of 53 ± 5 μm (not shown in the Figure) was determined, which is in accordance to our previous study.[11] Keeping the Fe-N-C loading comparable to the Pt-based CL loading requires a thicker CL due to their lower active site density.[3b] In a previous study we revealed a CL thickness of 66 ± 5 μm for a Pt-based CL with 40 wt% PTFE with a similar loading as the commercial GDE (0.76 mg_{Pt} cm^{-2} or 3.2 $mg_{Catalyst}$ cm^{-2}). In that study we have demonstrated that the CL thickness changes in correlation to the Pt loading.[11] As the Fe-N-C loading is in a comparable range in this study it is reasonable that the CL thicknesses are similar, while the 10 wt% PTFE displays a slight exception. For this GDE the fewest layers and thus less catalyst material was spray coated, resulting in this thinner CL. The 50 wt% PTFE CL establishes the lowest porosity of 3.1%, compared to the porosities of 9.2% (40 wt% PTFE), 10.9% (20 wt% PTFE) and 15.7% (10 wt% PTFE). While the CL thickness is similar for 20–50 wt%, the porosity decreases with increased PTFE content, indicating that the PTFE blends efficiently into the porous structure and generates a denser CL. Mack et al. described that Pt-based GDEs with 40 wt% PTFE showed a lower porosity in SEM analysis as well reduced surface conductivity (AFM conductivity mapping) compared to 5 and 10 wt% PTFE.[8a] Also, Liu et al. reported a decrease of surface area and pore volume with increasing PTFE

content (0, 10, 25 and 40 wt% PTFE) in the CL of Pt-based GDEs, determined by desorption analysis.[9a] Thus, in Pt-based literature studies it was revealed that more PTFE generates a more compact and less porous GDE morphology, which is in accordance to increased density (Figure 2-C) of the Fe-N-C CLs in this work. To firstly sum up, it was achieved to fabricate GDEs with comparable catalyst loading, homogenous distributed PTFE and catalyst particles on the CL as visible within the SEM/EDS images (Figure 1) and as well homogenously distributed PTFE inside the CL as no agglomerates are visible in the CL images (Figure 2).

Wettability of the CL surface

Contact angle analysis in Figure 3 displays the CLs wettability with H_2O and H_3PO_4. For the 10 wt% PTFE GDE the H_2O contact angle is significantly lower ($79 \pm 4°$) compared to the other GDEs with contact angles of around 150°. This originates from its lower hydrophobicity allowing more H_2O penetration into the CL because of this relatively low PTFE content. H_3PO_4 is used along with H_2O to get information of the wettability conditions in HT-PEMFC. H_3PO_4 contact angles of 10 wt% ($75 \pm 8°$) and 20 wt% PTFE ($86 \pm 6°$) are in a lower range compared to 40 and 50 wt% PTFE with H_3PO_4 contact angles of around 140°. The H_2O and H_3PO_4 contact angles of the 20 wt% PTFE GDE in Figure 3 exhibit significant deviation along each other in contrast to the other GDEs. This can be attributed to the Fe–N_x and N-functionalities, which are protonated in acidic environment and attract the phosphate anions (H_3PO_4 electrolyte) by coulombic interaction.[6,7b] The H_2O contact angle of the 20 wt% PTFE CL is higher, because obviously less interaction occurs, while this PTFE or lower contents are not able to counter-
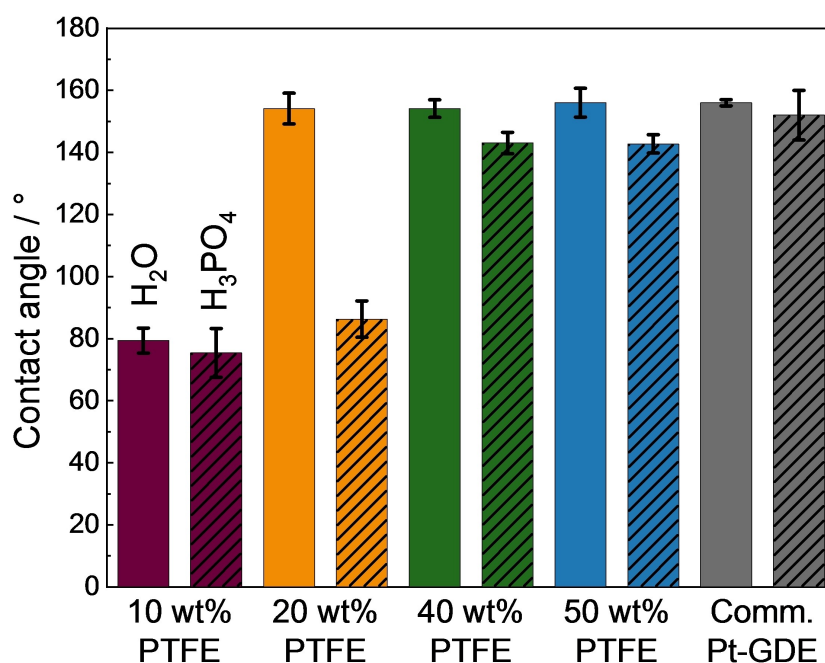

Figure 3. Contact angles of water and phosphoric acid (hatched bars/every second bar) with the CL, recorded at room temperature.

ChemElectroChem

Research Article
doi.org/10.1002/celc.202300583

Chemistry
Europe
European Chemical
Societies Publishing

balance the H_3PO_4 drag into the CL. PTFE contents above 20 wt% are able to diminish the acid drag and thus achieve increased acidophobic character a towards H_3PO_4. Contact angles reported by Halter et al. revealed that the wetting behavior of PTFE with conc. H_3PO_4 at 160 °C is similar to the wetting with H_2O at room temperature. The contact angle of H_3PO_4 increased with elevated temperature due to higher acid concentration.[14] Considering this, the H_3PO_4 wettability of the GDE with 20 wt% PTFE at 160 °C might be comparable to the 40 and 50 wt% PTFE GDEs.

For a sufficient proton transport an adequate amount electrolyte needs to cover the active $Fe-N_x$-sites without flooding the porous structure, which leads to gas transport inhibition.[6] The lower the contact angle the more electrolyte penetrates into the CL, which probably leads to flooding of the pores. The higher the contact angle the less electrolyte might be available for proton transport. To determine the optimal contact angle value for performance, the results are compared with Pt-based CLs. It is assumed that wettability similar to that of the benchmark Pt-based GDE is helpful for sufficient performance. In comparison to our results, a PTFE content of 18 wt% was already sufficient to achieve a contact angle of >140° for a Pt-based GDE in another study.[15] This contact angle is comparable to the commercial Pt-based GDE for HT-

PEMFC application, with values of $156 \pm 1°$ for H_2O and $152 \pm 8°$ for H_3PO_4 (Figure 3). These pronounced hydrophobic characteristic is needed to hinder acid flooding of the pores and prevent leakage, which is more important for the Pt-based GDE as the CL is thinner compared to Fe-N-C GDEs.[9d,15] The 40–50 wt% PTFE Fe-N-C-based GDEs display contact angles in a similar range. It seems that for achieving similar wettability to Pt-based CLs twice as much PTFE is required, when Fe-N-C catalyst is used. This reveals that due to the acidophilic character of Fe-N-C catalysts higher PTFE contents are required to achieve H_3PO_4 contact angles >140°. At least >20 wt% PTFE contents are needed to ensure sufficient hydrophobic properties. The impact on the electrochemical behavior is discussed in the following section.

GDE half-cell characterization under HT-PEMFC conditions

The effect of different PTFE contents in the CL on the ORR performance was investigated. For this, the GDEs were hot-pressed onto a phosphoric-acid doped polybenzimidazole membrane and mounted in a commercial GDE half-cell setup, with an operating temperature of 160 °C and conc. H_3PO_4 electrolyte. The ORR polarization curves are plotted in Figure 4-
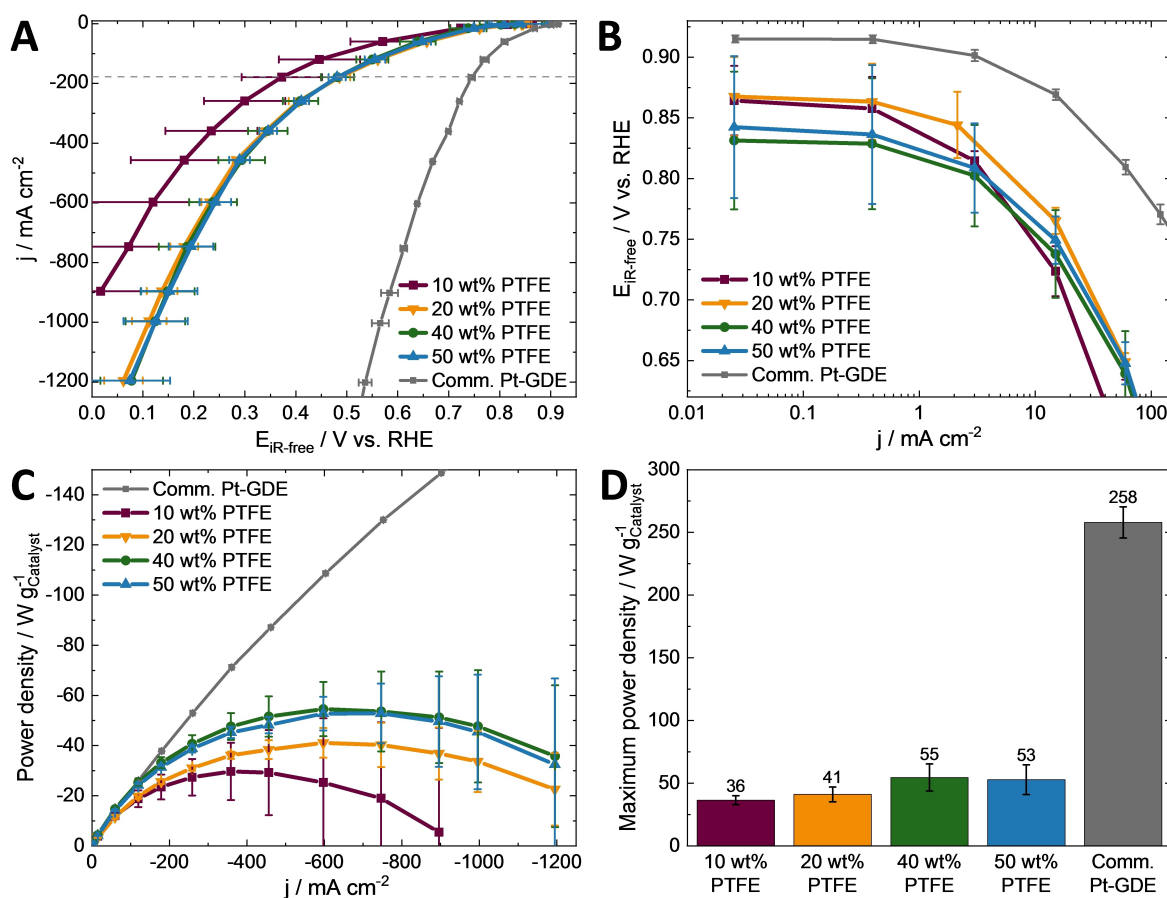

Figure 4. (A) Polarization curves of Fe–N–C based GDEs with varied PTFE amounts, (B) semi-logarithmic plots of the activation areas of the polarization curves, (C) power density curves normalized to ICP-MS catalyst loading and their maximum power densities (D). The measurement was conducted in a GDE half-cell setup (160 °C, oxygen flow rate 1.5 L min⁻¹, conc. H_3PO_4).

ChemElectroChem

Research Article
doi.org/10.1002/celc.202300583

Chemistry
Europe
European Chemical
Societies Publishing

A. Figure 4-B shows a semi-logarithmic plot of low current density region. For small current densities from 0.03 up to 3 mA cm^{-2} the Fe-N-C GDEs undergo comparable activation losses, which stem from the use of the same catalyst material in all GDEs here. However, Figure 4-A depicts that with increasing current densities ($>$60 mA cm^{-2}) the differences in half-cell performances more visible. For comparison, the polarization curve of the commercial Pt-based GDE is plotted in Figure 4-A, exhibiting -as expected- the highest performance. The 10 wt% PTFE GDE obviously suffers from a higher activation loss and ohmic loss compared to the other GDEs. The GDEs with 20, 40 and 50 wt% PTFE reach similar performances of 0.49 ± 0.02 V, 0.48 ± 0.03 V and 0.48 ± 0.02 V at 178 mA cm^{-2} (see dashed line in Figure 3-A). In contrast, the 10 wt% PTFE GDE shows a lower performance of 0.37 ± 0.1 V. To achieve high comparability between the GDEs the power density curves are normalized to the total catalyst loading (see Figure 1) and plotted in Figure 4-C as function of current density. Power density curves normalized to the geometric surface area are available in the supporting information in Figure S. 3. Among the Fe-N-C based GDEs, the highest power densities are reached with 40 and 50 wt% PTFE. The 20 wt% PTFE GDE power density progression is in close range. For the GDEs the power density reaches a maximum around 600–750 mA cm^{-2}. In comparison, the 10 wt% PTFE GDE reveals the lowest power density and already decays at lower current density of 360 mA cm^{-2}. For the Pt-based GDE no decrease in power density curve could be overserved. Therefore, the highest power density is used as maximum power (Figure 4-D) for comparison with the Fe–N–C power densities. For better visability of the Fe-N-C GDEs curves the Pt-based GDE power density curve is only partly shown (full curve in supporting information in Figure S3-E). Figure 4-D compares the maximum power densities of the curves from Figure 4-C. The 10 wt% PTFE GDE exhibits the lowest maximum power density of 36 ± 4 W g$_{Catalyst}^{-1}$. It is followed by the 20 wt% PTFE GDE with 41 ± 6 W g$_{Catalyst}^{-1}$, which comes close to the 40 and 50 wt% PTFE GDEs, which achieve similar maximum power densities of 55 ± 11 and 53 ± 12 W g$_{Catalyst}^{-1}$. The Pt-GDE reaches the highest power density of 258 ± 12 W g$_{Catalyst}^{-1}$. The reasons for the significant decrease in performance for PTFE contents below 20 wt% PTFE with increased ORR rate ($>$60 mA cm^{-2}) are the different wettability and morphology properties and will be disclosed in the following.

With increasing current density, more water is produced, which usually leads to diluting and rearranging of the phosphoric acid water mixture inside the porous structure.[7a] Depending on the CL structure and wettability properties it is important to create a thin film of electrolyte covering the catalyst structure while hindering the blocking of actives sites trough pore flooding or leaving actives sites inaccessible.[5a] A thick electrolyte film represents a high diffusion barrier for oxygen to the active Fe-N$_x$-sites as the oxygen solubility in phosphoric acid is low.[6] Flooding of the CL with product water and H$_3$PO$_4$ due to a more hydrophilic surface and stronger acid penetration (see Figure 3) cause lower performance of the 10 wt% GDE at current densities $>$60 mA cm^{-2} and also results in the lowest maximum power density around 360 mA cm^{-2}. The

strong acid drag due to acidophilic character of the Fe-N-C is observable by the contact angle analysis shown in Figure 3, where the 10 wt% PTFE GDE exhibits the lowest contact angle with H$_2$O of 79° compared to $>$150° for the 20, 40 and 50 wt% GDEs. The latter GDEs unveiled higher power densities with a maximum around 600–750 mA cm^{-2} (Figure 4-C) of comparable maximum power densities (Figure 4-D). This probably originates from their beneficial CL wetting characteristic, which counter-balances the electrolyte drag due to the Fe-N-C catalyst into the CL, and allows sufficient transport of the reactants to the active sites, compared to the 10 wt% PTFE GDE. GDEs with more than 20 wt% PTFE exhibit a hydrophobic CL with H$_2$O-based contact angles around 140-150°, which seems to be beneficial for the cell performance. It is noticeable that the H$_3$PO$_4$-based contact angle of the 20 wt% PTFE GDE is in the same range as the 10 wt% PTFE GDE (Figure 3). However, the 20 wt% PTFE GDE demonstrates a higher half-cell performance (Figure 4-A, -C). As described by Halter et al., the wettability of PTFE with H$_3$PO$_4$ at 160 °C is similar to H$_2$O at room temperature.[14] This agrees with the similar performance of the 20 to the 40 and 50 wt% PTFE GDEs, which established similar contact angles with H$_2$O (at room temperature) around 150°. The 10 wt% PTFE GDE owns the highest hydrophilic and acidophilic character, which agrees with the lowest performance due low oxygen access to the active sites caused by flooding. Additionally, μ-CT analysis (Figure 2) revealed the thinnest CL thickness of 80 ± 12 μm and less dense CL structure for the 10 wt% PTFE compared to the other GDEs, which might lead to increased acid penetration into the CL. Electrolyte flooding of the 10 wt% PTFE GDE results in high error bars for the polarization curve (Figure 4).

PTFE contents of at least 20 wt% provide a higher performance (Figure 4), because the flooding with electrolyte is impeded due to a more hydrophobic CL property and thus improves the access of the reactants to the active Fe-N$_x$-sites. Furthermore, flooding of the entire CL might be less pronounced, due to higher CL thickness (Figure 2-B). The performance and maximum power density remain relatively equal although the CL density increased with increased PTFE content (Figure 2-C). The GDEs with at least 20 wt% PTFE seem to have a more beneficial structure regarding the CL thickness and porosity as well as hydrophobicity in terms of formation of the three-phase boundary and catalyst utilization. The GDEs with 40–50 wt% PTFE exhibit highly comparable performances and maximum power densities, which shows that the catalyst material allows a wide range of PTFE contents with equal performance. Also, a higher PTFE content of 67 wt% was considered, however significant sedimentation of the catalyst suspension occurred, so that this PTFE amount is not applicable. Generally, it is a complex interplay between acid drag into the CL, optimal wetting of the mesoporous structure and hindering flooding to ensure high catalyst utilization.

The average ohmic resistance, determined by EIS for each of the polarization curves are 0.64 ± 0.1 Ω (10 wt%), 0.56 ± 0.02 Ω (20 wt%), 0.49 ± 0.05 Ω (40 wt%), 0.57 ± 0.05 Ω (50 wt%) and are plotted in the supporting information in Figure S. 4. In accordance to the ORR performance the slightly higher ohmic resistance and larger deviation for the 10 wt% PTFE GDE can be

ChemElectroChem

Research Article
doi.org/10.1002/celc.202300583

Chemistry Europe
European Chemical
Societies Publishing

assigned to flooding of the CL. The ohmic resistance remained relatively stable independent of applied current density, which can be seen in small error bars (supporting information Figure S4). Two measurements of the 10 wt% PTFE GDE showed a prominent decrease of resistance with increasing current density, leading to the high error bars. Overall the ohmic resistance is in a similar range for all measurements indicating comparability between the samples. Also, this demonstrates that the CL with different PTFE contents does not have a huge impact on the ohmic resistance, as the electric conductivity of the CL is only one contributor besides the electrolyte, MPL, GDL, contact plate.[16]

To gain insight into the electrochemical wettability of the CL, CVs were recorded before and after polarization curves. In Figure 5, the CVs normalized to the ICP-MS catalyst loading are shown. CVs normalized to the geometric area can be found in Figure S. 5 in the supporting information. Compared to the BoT CVs, a less tilted CV shape at EoT can be observed along all PTFE contents. This indicates enhanced wetting of the porous structure,[17] since water production during ORR leads to dilution of the electrolyte and redistribution of the phosphoric acid water mixture. There is no observable trend between the CVs shape or the electrochemical double layer capacitance. Redox peaks between 0.5 and 0.6 V are slightly visible for the 40 wt% GDE in Figure 5-G and can be attributed to hydroquinone/quinone species on the one hand and Fe^{2+}/Fe^{3+} redox transitions on the other hand, which are superimposed with the capacitive currents.[2] However, peaks around 0.2–0.4 V (anodic scan) are visible for the CVs in Figure 5-D–H. Similar peaks were observed in our previous studies.[2,18] Reason for this can be found in the investigation of Wang et al., which reveals a peak shift of iron redox couple of Fe-N-C catalyst to lower potentials in H_2SO_4 compared to $HClO_4$ electrolyte, due to lower adsorption strength of the corresponding anion with iron.[4c] As the adsorption strength of phosphate anions is smaller than sulphate anions[4c] the peak might be shifted even more to

lower potentials and explaining the peaks around 0.2–0.4 V. However, complete understanding remains unclear as literature about the behavior of Fe-N-C cathodes HT-PEM environment is lacking.

Also, the CVs experienced relatively high standard deviations between the measurements. 50 wt% PTFE inside the CL might lead to reduced electric conductivity as this GDE still experiences slightly shifted shape at EoT due to its high (non-electric conducting) PTFE content.[2] This could be the reason for the higher ohmic resistance compared to 20 and 40 wt% PTFE. CVs of the 10–40 wt% PTFE are not tilted any longer at EoT indicating that their less dense CL compared to 50 wt% PTFE (see Figure 2) enable adequate distribution of the viscous electrolyte. The same trend was also observed in the CVs with scan rates of 50 and 100 mV s^{-1} but less pronounced, therefore they are not shown here. Nevertheless, the polarization curves revealed a positive impact on performance above 20 wt% PTFE due to beneficial CL compactness and impeded flooding especially when applying higher current densities. The performance is not strongly impacted by the PTFE content, which demonstrates that the Fe-N-C catalyst can cope with a wide range of PTFE contents without compromising the performance. It is important to maintain a hydrophobic CL, wherefore at least 20 wt% PTFE are needed to counterbalance the acidophilic character of the catalyst material.

Conclusions

Fe-N-C-based GDEs with different PTFE contents of 10, 20, 40 and 50 wt% in the CL were studied under HT-PEMFC conditions in an electrochemical half-cell setup. The GDEs with 20, 40 and 50 wt% PTFE reach highly similar ORR performances, because they have sufficient hydrophobicity revealed by contact angles with water of $>140°$. The 10 wt% PTFE GDE demonstrates high attraction of water and H_3PO_4, is consequently more prone to
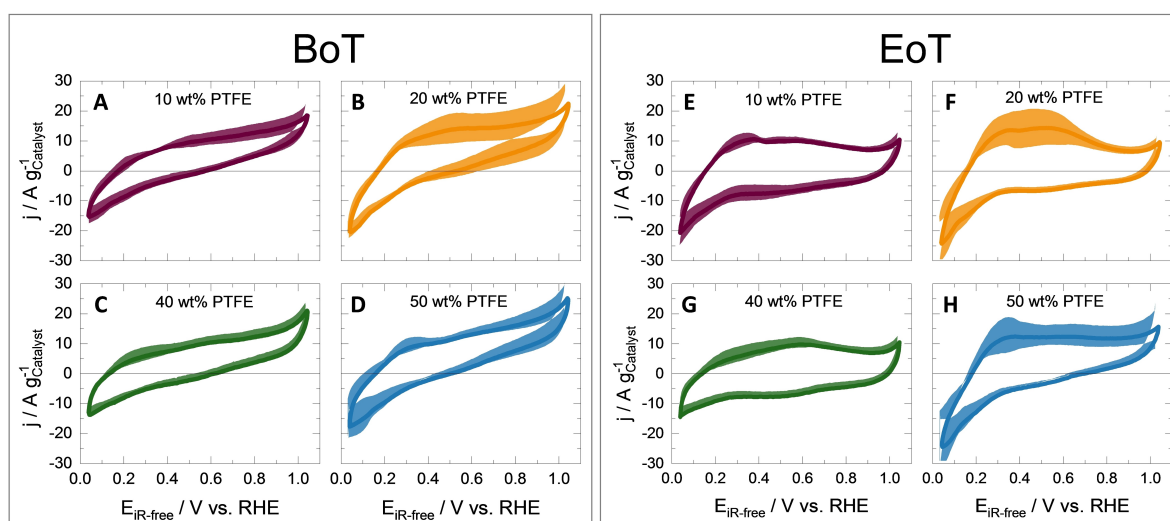

Figure 5. CVs recorded before (depicted in A–D as BoT) and after (depicted in E–H as EoT) recording of the polarization curve. The shade around each CV indicates the standard deviation between three independent measurements (for 50 wt% PTFE EoT only two CVs were recorded). The measurement was performed in a GDE half-cell at 160 °C, conc. H_3PO_4, Nitrogen flow rate of 120 mL min^{-1} and nitrogen purge of the electrolyte, scan rate 20 mV s^{-1}.

ChemElectroChem

Research Article
doi.org/10.1002/celc.202300583

Chemistry
Europe
European Chemical
Societies Publishing

flooding and discloses the lowest performance in comparison. μ-CT analysis revealed an increase in CL density with increased PTFE content, which has compared to the CL wettability a relatively low impact on the performance. This demonstrates that Fe-N-C catalyst can cope with a wide variety of CL compositions without compromising for the performance.

PTFE contents of at least 20 wt% generate similar hydrophobic characteristic of the CL like Pt-based GDEs and are needed for sufficient Fe-N-C GDE performance. This is in contrast to studies on Pt-based GDEs, where 5–20 wt% PTFE was shown to be optimal in HT-PEMFCs for enhanced wettability of the CL. Comparable properties of Fe-N-C to Pt-based GDEs appear to be beneficial for performance, whereas higher PTFE contents are required. This study discloses that, different to Pt-based GDEs, Fe-N-C-based GDEs require higher PTFE contents to counterbalance the stronger acid attraction due to the more acidophilic Fe-N-C character. The highest performances are achieved with PTFE contents of 40–50 wt%. These PTFE contents seem to form a CL with proper wetting characteristic, thickness and porosity for appropriate transport of reactants to the active Fe-N$_x$-sites, while CVs and EIS indicate that the 50 wt% PTFE CL might suffer from slightly lower electric and proton conductivity.

The GDE half-cell performance, wettability and morphology results provide the basis for further development of Fe-N-C-based membrane-electrode-assemblies and testing in HT-PEM single cells. Conditioning of the Fe-N-C GDEs with an appropriate protocol, analysis of in-situ electrolyte distribution and examination of PTFE contents between 20 and 50 wt% in small increments should be considered for further studies. Generally, in order to create an adequate comparison of the performance of Fe-N-C GDEs to Pt-based GDEs, different CL PTFE contents should be considered to generate similar wetting properties. For further studies various Fe–N–C CL compositions (modified by catalyst ink viscosity, -additives, alternative binder, GDE thermal treatment) as well as other coating techniques like doctor blade coating should be investigated to disclose effects on performance. PTFE contents of 40–50 wt% could contribute to prevent acid leaching from the fuel cell and thus positively impact the fuel cell stability.

Experimental section

GDE fabrication

A commercial Fe-N-C catalyst (PMF-D14401, Pajarito Powder) was used for GDE fabrication. The catalyst powder was mixed with ultrapure water and 2-propanol (composition see Table 1), sonicated for 15 min using an ultrasonic (US) horn (amplitude 15%, on: 30 s, off: 10 s) while keeping the suspension cooled in an ice-bath. This suspension was then mixed on a roller mixer RS-TR 10 (Phoenix Instrument) overnight. Afterwards, it was sonicated in an ice-cooled US-bath for 10 min, followed by addition of PTFE-dispersion according to Table 1. The mixture was horn-sonicated (same conditions) and immediately transferred to the US spray coating device ExactaCoat (Sono-Tek) equipped with a 48 kHz nozzle. A gas diffusion layer (GDL) with microporous layer (MPL) (H23C2, Freudenberg) served as substrate and was placed on a heating plate at a temperature of 40 °C. The catalyst suspension was sprayed on an area of 5×5 cm² layer by layer in serpentine shape (rotated by 90° after each layer) with a flow rate of 0.2 mL min^{-1} including a drying step with nitrogen gas flow after each layer. The suspension was sonicated within its reservoir during the drying step. The targeted Fe-N-C loading was 3 mg$_{Catalyst}$ cm^{-2} for each GDE. For higher PTFE amounts the PTFE/catalyst ratio increased. Therefore, more coating layers (Table 1) were needed with increasing PTFE amount to keep the Fe-N-C loading in a comparable range. The GDEs were stored under nitrogen atmosphere until use.

Physical analyses

Determination of catalyst loading by inductively coupled plasma mass spectrometry

To examine the iron and platinum content in the GDEs inductively coupled plasma mass spectrometry (ICP-MS) was conducted with the iCap or XSeries2 device (Thermo Fisher Scientific). Alongside to 15 mg Fe-N-C catalyst, for each Fe-N-C GDE a 1 cm² piece was punched out, digested in 2 mL concentrated HNO$_3$ (Rotipuran®Supra 69 wt%, Carl Roth) and boiled at 100 °C for 1 h. The solution was stored overnight. Then, the sample was filtrated and the filtrate volume was adjusted to 50 mL by addition of ultrapure water. 10 μL of a scandium internal standard (1,000 mg L^{-1}, Carl Roth) was added to 10 mL of the sample solution. The calibration solutions consist of a Fe ICP standard (Carl Roth) with concentrations of 0; 5; 10; 20; 500; 1,000; 2,000 and 3,000 μg L^{-1}. A correlation coefficient of at least 0.999 was ensured during calibration. The Fe-N-C loading was calculated by correlating the iron content of the catalyst powder to the determined iron content of the CL.

A cross section of 8 mm from the commercial Celtec® Pt-based GDE was digested in a solution of 1.6 mL concentrated HCl (Rotipuran®Supra 30%, Carl Roth) in an ultra-sonic bath for 5–10 min.

Table 1. Composition of the catalyst suspension and GDE notation.

GDE notation	10 wt% PTFE	20 wt% PTFE	40 wt% PTFE	50 wt% PTFE
Catalyst/wt%	90	80	60	50
PTFE/wt%	10	20	40	50
PTFE/catalyst ratio	0.11	0.25	0.68	1.00
Solid/liquid ratio	Constant at 2.90			
Water/2-propanol ratio	Constant at 0.25			
Number of coating layers	168	188	240	298

ChemElectroChem

Research Article
doi.org/10.1002/celc.202300583

Chemistry
Europe
European Chemical
Societies Publishing

Afterwards, 1.2 mL concentrated HNO_3 (Rotipuran® Supra 69%, Carl Roth) was added (aqua regia dissolution). On the next day, the mixture was filtered and diluted to a total volume of 250 mL with 2% HNO_3 (Rotipuran® Supra 35%, Carl Roth) diluted by a factor of 5, acidified with 0.3 mL HNO_3 and further an internal Lutetium-Standard (final concentration $1\,mg\,L^{-1}$) was added. Calibration solutions for Pt were prepared with concentrations of 100, 200, 400, 600 and $800\,\mu g\,L^{-1}$. Each solution also contained a concentration of $1\,mg\,L^{-1}$ Lutetium as internal standard. Three platinum isotopes 194Pt, 195Pt und 196Pt were detected and averaged to calculate the final Pt concentration. Calibrations with a correlation coefficient of at least 0.999 were used for data evaluation.

Physico-chemical characterization

The surface morphology and elemental composition of the GDE surface was analyzed with SEM and EDS. GDEs pieces of about 0.5×0.5 cm were placed onto carbon tape on an aluminum sample holder and placed in the SEM Hitachi S-3200 N (Hitachi Ltd.) for acquiring of the SEM micrographs. The microscope was operated at an acceleration voltage of 20 kV in high vacuum. The EDS mapping of the GDE surface were performed with the equipped Oxford INCA EDS spectrometer (Oxford Instruments) and the spectra were analyzed within the INCA software (Oxford Instruments). The EDS results of the fluorine, carbon and iron elemental composition mapping of an area of roughly 107×156 μm at two different positions of the GDE surface were averaged. The fluorine amounts are used to estimate the PTFE content in der CL surface. A composition of C_2F_4 is assumed so that a part of the detected carbon is attributed to the PTFE.

GDE pieces with a diameter of 6 mm were punched out and vertically placed in the μ-CT SkyScan 1172 (Bruker). Table 2 shows the experimental parameters during measurement. The reconstruction was performed with NRecon software (Bruker) and a volume of interest (VOI) was extracted using the software DataViewer (Bruker) to generate 2D images of the GDE. For determining the CL thickness, the whole GDE thickness at 30 positions was determined at two representative cross sections using DataViewer software (Bruker) first. Afterwards the GDL/MPL width – determined in the same way from Freudenberg H23C2 GDL/MPL without the presence of CL – was subtracted from the GDE thickness to finally receive the CL thickness. 3D images were received using the software CT_{Vox} (Bruker). The porosity was determined in the CT_{An} software (Bruker) from binarized images by calculating the proportion of the structure to the void of the total VOI. The size of the voxels is given by the resolution of the μ-CT measurement ($1.9\,\mu m\,pxl^{-1}$) so that only the large macropores will be captured by this analysis and the smaller pores are not considered.

Contact angle

Contact angle measurements were carried out with the device OCA25 (Dataphysics). Drops (10 μL) of ultrapure water or conc. phosphoric acid (85 vol% H_3PO_4 Emsure® Merck) were deposited via a blunt cannula onto the CL of a horizontal aligned GDE under ambient conditions. For water a cannula of 0.26 mm and for conc. phosphoric acid of 0.60 mm inner diameter was used. Analysis of contact angles was done using Young-Laplace fitting within dpiMAX Software (Dataphysics). The H_2O and H_3PO_4 contact angles of six independent measurement points were averaged for each electrode.

GDE/membrane assembling

With a two-pillar press TRG-2 (P/O/Weber) a phosphoric-acid doped polybenzimidazole membrane Celtec®-P (BASF) was hot pressed with 1 kN for 30 s at 140°C with the CL side of the GDE. The membrane was stored several days in 50 vol% H_3PO_4 before use. Shim shields of around 80% of the initial thickness of the GDE and membrane protected the GDE/membrane from crushing. Afterwards the GDE/membrane was fixed in the half-cell being ready for measurements.

GDE half-cell measurements

The half-cell measurements were performed in a commercially available setup FlexCell® PTFE (Gaskatel). The cell construction was modified with a PTFE shield to give a limited geometric active area of 0.785 cm², saving material and enabling higher current densities. Furthermore, a copper plate leaving the geometric active area free was placed on the GDL-side of the GDE to enhance electrical conductivity. The GDE (working electrode, WE), the copper plate and the PTFE shield were sandwiched between two silicon sealings and placed between the electrolyte and gas compartment (supporting information, Figure S6). After cell assembling, the gap between the two cell compartments was sealed with PTFE tape to prevent unwanted gas penetration to the GDE. 40 mL of conc. phosphoric acid (85% H_3PO_4 Emsure® Merck) served as electrolyte. As counter electrode (CE) a Pt coil and as reference electrode a reversible hydrogen electrode (RHE) (Gaskatel), which was frequently calibrated against a H_2/Pt electrode, were used. The cell was heated to 160°C with heating elements inside the cell body regulated by the temperature control box (Gaskatel). Before the measurements, all compartments were rinsed with ultrapure water and 2-propanol ($\geq 99.5\%$ for synthesis, Carl Roth) and dried.

Electrochemical measurements were performed using the potentiostat Modulab2100 A (Ametek) equipped with a 12 V/20 A external booster (Ametek). Cyclic voltammograms (CVs) were recorded as follows. Nitrogen with a flow rate of 120 mL min⁻¹ was led through the gas compartment starting 15 min before and maintained during CV recording. Simultaneously, nitrogen was led into the electrolyte compartment to remove and keep the electrolyte free from oxygen. The CV-procedure consists of three cycles for each scan rate of 20, 50 and 100 mV s⁻¹ between 0.05 and 1.05 V_{RHE}. An electrochemical impedance spectrum (EIS) from 0.1 Hz to 300 kHz at 0.5 V_{RHE} with an amplitude of 0.01 V was recorded, where the uncompensated resistance (R_u) was extracted at the intercept with the x-axis or the minimum. The CVs were recorded again with same parameters but with in-situ compensation of the iR-drop of 95%. These CVs were recorded before the polarization curves and assigned as "begin of test" (BoT) CVs. With the same parameters CVs were recorded after polarization curve measurement and assigned as "end of test" (EoT) CVs. The measurement protocol for polarization curves was adapted from Ehelebe et al.[16] First, oxygen

Table 2. Experimental parameters of μ-CT measurements.	
Parameter/unit	Value
Acceleration voltage/kV	80
Current/μA	100
Rotation step/°	0.2
Random movement	4
Averaging frames	10
Resolution/$\mu m\,pxl^{-1}$	1.9
Exposure time/ms	1450
Stage temperature/°C	Room temperature

with a flow rate of 1.5 L min^{-1} was led through the gas compartment of the cell for at least 20 min or until stable (fluctuation < 0.1 mV) open circuit potential for more than five minutes. Galvanostatic steps are applied for 30 s for currents (i) from -0.03 mA to -460 mA and for 5 s from -0.6 A to -2.0 A. The shorter holding time was chosen to minimize the increase in temperature due to the higher reaction rates. Each current step was directly followed by EIS at the same current density. The frequency range was set in a range from 0.1 Hz to 300 kHz with amplitudes from 1 up to 800 mA and increases with increasing current density. The last 3 s of the recorded potential at each current step were averaged and afterwards iR-drop (R extracted from EIS) corrected ($E_{iR\_corrected} = E_{uncompensated} - i*R$).

Supporting Information

Supporting Information to this article is available online.

Conflict of Interests

The authors declare no conflict of interest.

Data Availability Statement

The data that support the findings of this study are available from the corresponding author upon reasonable request.

[1] Q. Meyer, C. Yang, Y. Cheng, C. Zhao, *Electrochem. Energy Rev.* **2023**, *6*.
[2] J. Müller-Hülstede, T. Zierdt, H. Schmies, D. Schonvogel, Q. Meyer, C. Zhao, P. Wagner, M. Wark, *J. Power Sources* **2022**, *537*, 231529.
[3] a) N. Seselj, S. M. Alfaro, E. Bompolaki, L. N. Cleemann, T. Torres, K. Azizi, *Adv. Mater.* **2023**, ■■■*Dear Author, if the journal has volumes, please add the journal number*■■■; b) L. Osmieri, Q. Meyer, *Curr. Opin. Electrochem.* **2022**, *31*.
[4] a) Y. Hu, J. O. Jensen, C. Pan, L. N. Cleemann, I. Shypunov, Q. F. Li, *Appl. Catal. B* **2018**, *234*, 357–364; b) K. Holst-Olesen, M. Reda, H. A. Hansen, T. Vegge, M. Arenz, *ACS Catal.* **2018**, *8*, 7104–7112; c) X. P. Wang, M. Ferrandon, J. H. Park, J. J. Shen, A. J. Kropf, H. G. Zhang, P. Zelenay, D. J. Myers, *Electrochim. Acta* **2023**, *443*.
[5] a) N. Bevilacqua, T. Asset, M. A. Schmid, H. Markötter, I. Manke, P. Atanassov, R. Zeis, *J. Power Sources Adv.* **2021**, *7*, 100042 (100041–100049); b) M. Primbs, Y. Y. Sun, A. Roy, D. Malko, A. Mehmood, M. T. Sougrati, P. Y. Blanchard, G. Granozzi, T. Kosmala, G. Daniel, P. Atanassov, J. Sharman, C. Durante, A. Kucernak, D. Jones, F. Jaouen, P. Strasser, *Energy Environ. Sci.* **2020**, *13*, 2480–2500; c) D. Malko, T. Lopes, E. A. Ticianelli, A. Kucernak, *J. Power Sources* **2016**, *323*, 189–200.
[6] N. Pimperl, N. Bevilacqua, M. A. Schmid, P. A. L. Torres, H. A. El-Sayed, R. Zeis, K. P. Zeyer, *J. Power Sources* **2021**, *507*.
[7] a) N. Bevilacqua, R. Gokhale, A. Serov, R. Banerjee, M. Schmid, P. Atanassov, R. Zeis, *ECS Trans.* **2018**, *86*, 221–229; b) J. Müller-Hülstede, L. M. Uhlig, H. Schmies, D. Schonvogel, Q. Meyer, Y. Nie, C. Zhao, J. Vidakovic, P. Wagner, *ChemSusChem* **2023**, *16*, e202202046.
[8] a) F. Mack, T. Morawietz, R. Hiesgen, D. Kramer, R. Zeis, *Polym. Electrolyte Fuel Cells* **2013**, *58*, 881–888; b) F. Mack, M. Klages, J. Scholta, L. Jorissen, T. Morawietz, R. Hiesgen, D. Kramer, R. Zeis, *J. Power Sources* **2014**, *255*, 431–438; c) S. Kim, T. D. Myles, H. R. Kunz, D. Kwak, Y. Wang, R. Maric, *Electrochim. Acta* **2015**, *177*, 190–200.
[9] a) S. Liu, K. Wippermann, W. Lehnert, *Int. J. Hydrogen Energy* **2021**, *46*, 14687–14698; b) P. Mazur, J. Soukup, M. Paidar, K. Bouzek, *J. Appl. Electrochem.* **2011**, *41*, 1013–1019; c) G. Jeong, M. Kim, J. Han, H. J. Kim, Y. G. Shul, E. Cho, *J. Power Sources* **2016**, *323*, 142–146; d) F. Mack, T. Morawietz, R. Hiesgen, D. Kramer, V. Gogel, R. Zeis, *Int. J. Hydrogen Energy* **2016**, *41*, 7475–7483.
[10] a) Y. Cheng, S. He, S. F. Lu, J. P. Veder, B. Johannessen, L. Thomsen, M. Saunders, T. Becker, R. De Marco, Q. F. Li, S. Z. Yang, S. P. Jiang, *Adv. Sci.* **2019**, *6*, 1802066 (1802061–1802068); b) F. Razmjooei, J. H. Yu, H. Y. Lee, B. J. Lee, K. P. Singh, T. H. Kang, H. J. Kim, J. S. Yu, *ACS Appl. Energ. Mater.* **2020**, *3*, 11164–11176; c) Y. Cheng, J. Y. Zhang, X. Wu, C. J. Tang, S. Z. Yang, P. P. Su, L. Thomsen, F. P. Zhao, S. F. Lu, J. Liu, S. P. Jiang, *Nano Energy* **2021**, *80*; d) R. Gokhale, T. Asset, G. Qian, A. Serov, K. Artyushkova, B. C. Benicewicz, P. Atanassov, *Electrochem. Commun.* **2018**, *93*, 91–94; e) A. Byeon, K. J. Lee, M. J. Lee, J. S. Lee, I. H. Lee, H. Y. Park, S. Y. Lee, S. J. Yoo, J. H. Jang, H. J. Kim, J. Y. Kim, *ChemElectroChem* **2018**, *5*, 1805–1810; f) K. Strickland, R. Pavlicek, E. Miner, Q. Y. Jia, I. Zoller, S. Ghoshal, W. T. Liang, S. Mukerjee, *ACS Catal.* **2018**, *8*, 3833–3843; g) Y. Hu, J. O. Jensen, W. Zhang, S. Martin, R. Chenitz, C. Pan, W. Xing, N. J. Bjerrum, Q. F. Li, *J. Mater. Chem. A* **2015**, *3*, 1752–1760.
[11] H. Schmies, T. Zierdt, J. Müller-Hülstede, W. Deter, J. Lorenz, M. Wark, P. Wagner, *J. Power Sources* **2022**, *529*, 231276.
[12] Y. X. Zhao, G. F. Zhao, Y. D. Jiang, *Int. J. Fract.* **2013**, *183*, 63–80.
[13] A. A. Samu, I. Szenti, A. Kukovecz, B. Endrodi, C. Janaky, *Commun. Chem.* **2023**, *6*.
[14] J. Halter, T. Gloor, B. Amoroso, T. J. Schmidt, F. N. Buchi, *Phys. Chem. Chem. Phys.* **2019**, *21*, 13126–13134.
[15] H. S. Jung, D. H. Kim, H. Chun, C. Pak, *J. Ind. Eng. Chem.* **2022**, *109*, 267–274.
[16] K. Ehelebe, D. Seeberger, M. T. Y. Paul, S. Thiele, K. J. J. Mayrhofer, S. Cherevko, *J. Electrochem. Soc.* **2019**, *166*, F1259–F1268.
[17] a) H. Y. Liu, K. P. Wang, H. S. Teng, *Carbon* **2005**, *43*, 559–566; b) N. Pilinski, N. K. Nagappan, B. Satola, M. Rastedt, A. Dyck, P. Wagner, *ECS Trans.* **2018**, *86*, 315–327.
[18] J. Müller-Hülstede, H. Schmies, D. Schonvogel, Q. Meyer, Y. Nie, C. Zhao, P. Wagner, M. Wark, *Int. J. Hydrogen Energy* **2023**, *50*, 921–930.

RESEARCH ARTICLE
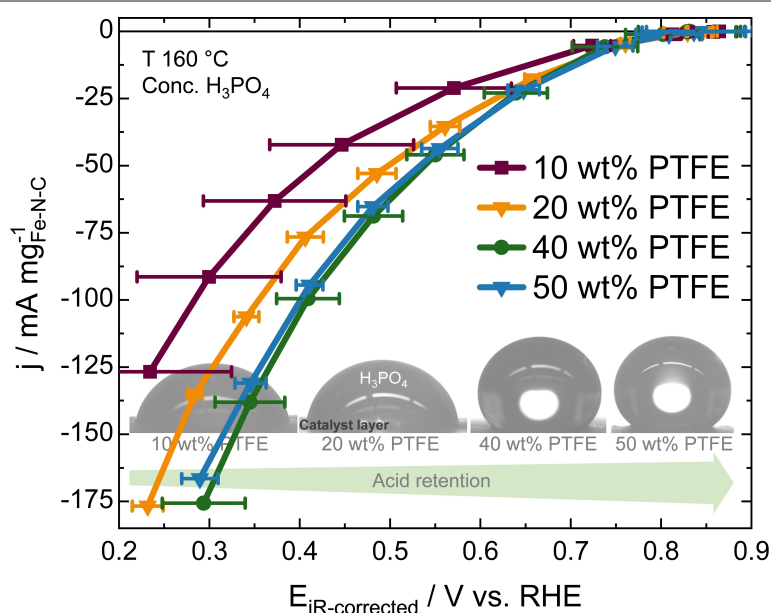
T. Zierdt*, Dr. J. Müller-Hülstede, Dr. H. Schmies, Dr. D. Schonvogel, P. Wagner, Prof. Dr. K. A. Friedrich

1 – 12

Effect of Polytetrafluorethylene Content in Fe−N−C-Based Catalyst Layers of Gas Diffusion Electrodes for HT-PEM Fuel Cell Applications

Platinum-based electrodes are cost-intensive and partly poisoned by phosphate ions (proton conductor) in the high temperature polymer electrolyte membrane fuel cell (HT-PEMFC). Fe-N-C-based electrodes do not contain noble metals and are not poisoned by phosphate ions. These catalysts show sufficient performance, however are still outperformed and less stable compared to Pt-catalyst in HT-PEMFC cells. Therefore, investigation of Fe-N-C electrodes is necessary.

ORCID (Open Researcher and Contributor ID)

Please check that the ORCID identifiers listed below are correct. We encourage all authors to provide an ORCID identifier for each coauthor. ORCID is a registry that provides researchers with a unique digital identifier. Some funding agencies recommend or even require the inclusion of ORCID IDs in all published articles, and authors should consult their funding agency guidelines for details. Registration is easy and free; for further information, see http://orcid.org/.

Tanja Zierdt http://orcid.org/0000-0003-1527-199X
Dr. Julia Müller-Hülstede
Dr. Henrike Schmies http://orcid.org/0000-0002-6565-1280
Dr. Dana Schonvogel http://orcid.org/0000-0002-2485-740X
Peter Wagner http://orcid.org/0000-0002-5644-9881

Prof. Dr. K. Andreas Friedrich http://orcid.org/0000-0002-2968-5029